LAWRENCE
LIVERMORE
NATIONAL
LABORATORY

LLNL-PROC-420848

Development of Ta-based Superconducting Tunnel Junction X-ray Detectors for Fluorescence XAS

S. Friedrich, O. Drury, J. Hall, R. Cantor

December 1, 2009

13th International Synchrotron Radiation Instrumentation Conference
Melbourne, Australia
September 28, 2009 through October 2, 2009

Disclaimer

Development of Ta-based Superconducting Tunnel Junction X-ray Detectors for Fluorescence XAS

Stephan Friedrich[a], Owen B. Drury[a], John Hall[b], and Robin Cantor[b]

[a]*Lawrence Livermore National Lab, Advanced Detector Group, 7000 East Ave., L-188, Livermore, CA 94550, USA*
[b]*STAR Cryoelectronics, 25-A Bisbee Court, Santa Fe, NM 87508, USA*

Abstract. We are developing superconducting tunnel junction (STJ) soft X-ray detectors for chemical analysis of dilute samples by fluorescence-detected X-ray absorption spectroscopy (XAS). Our 36-pixel Nb-based STJ spectrometer covers a solid angle $\Omega/4\pi \approx 10^{-3}$, offers an energy resolution of ~10-20 eV FWHM for energies up to ~1 keV, and can be operated at total count rates of $\sim 10^6$ counts/s. For increased quantum efficiency and cleaner response function, we have now started the development of Ta-based STJ detector arrays. Initial devices modeled after our Nb-based STJs have an energy resolution below 10 eV FWHM for X-ray energies below 1 keV, and pulse rise time discrimination can be used to improve their response function for energies up to several keV. We discuss the performance of the Ta-STJs and outline steps towards the next-generation of large STJ detector arrays with higher sensitivity.

Keywords: Superconducting tunnel junctions, STJ X-ray detectors, X-ray absorption spectroscopy
PACS: 07.85.Qe, 07.85.Nc, 61.10.Ht, 85.25.Oj, 78.70.En

INTRODUCTION

Superconducting tunnel junctions (STJs) are being developed as energy-dispersive soft X-ray detectors, because they combine the high energy resolution of low-temperature detector technology with the comparably high count rate capabilities of non-thermal devices [1]. In synchrotron science, these characteristics make STJ X-ray detectors attractive to study the chemistry of dilute samples by fluorescence-detected X-ray absorption spectroscopy (XAS). STJs are preferred whenever silicon or germanium detectors lack energy resolution, and grating spectrometers lack efficiency. In practice, this means STJs are favored for fluorescence-detected XAS in the soft X-ray band below ~1 keV where the light-element K-edges and transition metal L- and M-edges lie [2].

The most mature superconducting devices today are based on niobium (Nb) and aluminum (Al) films. Nb is often preferred because it is the elemental superconductor with the highest critical temperature $T_C(\mathrm{Nb}) \approx 9$ K and thus enables device operation in a liquid He bath at 4.2 K. Al is favored because it grows a comparably rugged oxide Al_2O_3 that can provide a high-quality pinhole-free tunnel barrier. Nb-Al junction technology was developed in the 1980's when superconducting logic was considered a viable alternative to supersede Si-based circuitry, and the Nb-based STJ detectors we have been using are a direct outgrowth of this effort. Our detectors have achieved an energy resolution between ~2 eV FWHM at 70 eV and ~9 eV FWHM at 1 keV [3], and have been operated successfully at the ALS synchrotron at count rates up to ~30,000 counts/s per pixel since 2001 [4]. However, for X-ray detection Nb is not the ideal material. Its moderately low atomic number $Z_{\mathrm{Nb}} = 41$ translates into only moderate absorption efficiency, and produces a line-splitting artifact that limits operation of Nb-based STJs to energies below ~1 keV. In addition, devices with lower T_C have smaller energy gaps Δ and thus offer potentially higher energy resolution. Tantalum (Ta) and lead (Pb) based STJ detectors have been built, with a resolution between 2.6 eV FWHM at 400 eV [5] and 12 eV at 6 keV [6], but their design led to slower pulses that were less suitable for synchrotron science.

We have now started an effort to develop STJ X-ray detectors based on Ta-Al thin film technology. The devices were fabricated at STAR Cryoelectronics, and tested at Lawrence Livermore National Laboratory. Here we present the characteristics of initial Ta-based STJ detectors that were modeled after our current Nb-based devices, and discuss their dc and pulse detection characteristics. The results suggest future modifications in the detector design to further improve the sensitivity of STJ spectrometers for synchrotron science.

TANTALUM VS. NIOBIUM-BASED STJ DETECTORS

STJ X-ray detectors consist of two superconducting electrodes separated by a thin insulating tunnel barrier. X-rays absorbed in one of the electrodes excite free charge carriers ("quasiparticles") above the superconducting energy gap Δ in proportion to their energy, and the resulting increase in tunneling current provides a direct measure of the X-ray energy (fig. 1a). The small (~meV) energy gap translates into high energy resolution, and the short (~μs) quasiparticle recombination time τ_{rec} ensures count rate capabilities above 10,000 counts/s per STJ detector pixel. For increased efficiency, a low-gap superconductor (usually Al) is used to trap quasiparticles from the absorber into a volume close to the tunnel barrier. Quasiparticle can tunnel multiple times at a rate $1/\tau_{tun}$ until they recombine after τ_{rec}, each transferring charge in the same forward direction and thus increasing the signal charge by a factor $\langle n \rangle = \tau_{rec}/\tau_{tun}$ (fig. 1a, green arrows). Quasiparticles that have not scattered below $\Delta + eV_{bias}$ in the electrodes can also tunnel against the bias, thereby reducing the signal and adding noise (fig. 1a, red arrow). Statistical fluctuations in charge generation and tunneling limit the energy resolution of STJs to

$$\Delta E_{FWHM} = 2.355\sqrt{\varepsilon E_x\left(F+1+\frac{1}{\langle n\rangle}+\frac{4\gamma(1-\gamma)}{(1-2\gamma)^2}\right)}. \qquad (1)$$

Here $\varepsilon \approx 1.7\Delta$ is the energy to create a single excess quasiparticle [7], F = 0.2 is the Fano factor that describes the fluctuation in the initial charge generation [7], $1+1/\langle n \rangle$ accounts for the noise due to charge multiplication [8], and γ is the fraction of quasiparticles above $\Delta+eV_{bias}$ that can tunnel against the bias [9].

Nb-based STJs tend to suffer from the fact that one of the native oxides (NbO) is a superconductor with a low critical temperature $T_C(NbO) \approx 0.5$ K whose small gap traps quasiparticles away from the tunnel barrier (fig.1a, red arrow). Surface oxides thus lead to a shorter quasiparticle recombination time τ_{rec}, a reduced signal and increased noise (eq. 1). In addition, the energy gap in tantalum $\Delta_{Ta} = 0.7$ meV is smaller than the gap in niobium $\Delta_{Nb} = 1.55$ meV, and Ta-based STJs can therefore have a ~50% higher energy resolution. But most importantly for synchrotron science, Ta is preferred because its high atomic number $Z_{Ta} = 73$ extends the energy range of operation, and reduces X-ray absorption in the bottom electrode that leads to a line splitting artifact [8, 10]. The drawbacks of Ta are that that the ~2× lower energy gap requires a ~2× lower operating temperature to reduce the thermal leakage current, and that the longer quasiparticle recombination time τ_{rec} reduces the maximum count rate.

As a first test, we have fabricated a set of Ta-based STJ detectors with the same nominal characteristics as the Nb-based STJ detectors that have produced the best results in our work since the 1990s [11, 3, 12]. They consist of a 265 nm Ta bottom film, an Al-AlOx-Al tunnel junction with 50 nm Al traps, and a top 165 nm Ta X-ray absorber. The goal was to produce junctions with small leakage current I_{bias} and high dynamic resistance R_{dyn} for low shot noise $(2eI_{bias})^{1/2}$ and low FET noise contribution $e_{n,FET}/R_{dyn}$ [13]. The devices were cooled to <0.1 K in an adiabatic demagnetization refrigerator (ADR) and exposed to X-rays from a two-stage X-ray tube. Figures 1b and 1c show the dc I(V) characteristics for a Nb and Ta STJ of similar size (blue), and their responsivity as a function of bias (red).

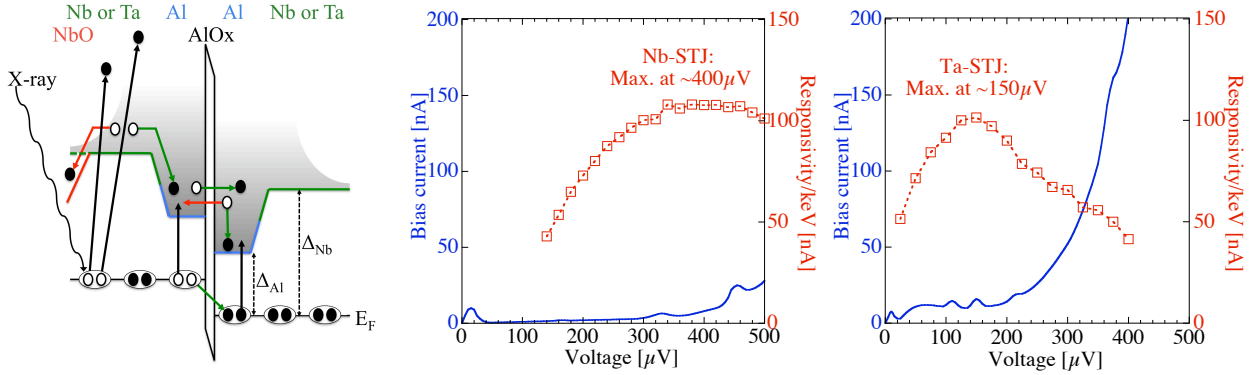

FIGURE 1. (a) The band diagram illustrates charge flow in an STJ. Quasiparticles excited above the gap Δ in the Nb or Ta absorber are trapped into the Al by inelastic scattering, and produce a current signal by tunneling across the barrier (green arrows). NbO at the detector surface produces unwanted trapping sites, and quasiparticles above Δ+eV can tunnel against the bias (red arrows). The density of quasiparticle states (grey) diverges at the gap. (b) Signal vs. bias in a 70 × 70 μm^2 Nb STJ. (c) Signal vs. bias in a 67 × 67 μm^2 Ta STJ. Both Nb and Ta STJs have a 165 nm top absorber film, a 265 bottom film, and 50 nm Al traps.

For voltages $V_{bias} < \Delta$, the dc bias current increases roughly exponentially as expected for negligible thermal currents, with a residual dc Josephson current close to V = 0 and several Fiske mode resonances at higher voltages. Since the Ta energy gap Δ_{Ta} is smaller than Δ_{Nb} and the Al gap is therefore smaller in the Ta-STJ due to the proximity effect, its leakage current increases at a lower voltage. But in contrast to Nb-based STJs, whose I(V) characteristics remain stable over many days during operation, the dc current in Ta-STJs can vary between different demagnetization cycles. This is, despite cryoperm shields around the ADR magnet and the STJ detector, likely due to magnetic flux trapping in the Ta films, which go through the superconducting transition around ~4 K when the magnetic field of the ADR is near its peak of ~4 T. The limiting leakage current, i.e. the current with the least amount of trapped flux, generally increases with Ta-junction size as expected, e.g. from ~2 nA for $(25\mu m)^2$ STJs to ~15 nA for the $(67\mu m)^2$ STJ and to ~150 nA for $(138\mu m)^2$ STJs at V_{bias} = 200 µV. But the variability of the leakage makes it difficult to assess whether it is due to imperfections of the tunnel barrier or trapped flux (in which case the leakage should roughly scale with area), or leakage along the junction edges (in which case it should roughly scale with circumference). In either case, these Ta STJs have sufficiently low leakage currents for low noise operation, with a measured current noise between ~0.2 and ~0.4 pA/√Hz for frequencies below 100 kHz.

For Nb- and Ta-STJs the response to X-rays changes as a function of bias voltage V_{bias} (figures 1b and 1c). Two competing effects contribute to this observation. One is that quasiparticles that have not scattered below $\Delta+eV_{bias}$ in the Al traps can tunnel both with and against the bias (fig. 1a). As V_{bias} is increased, the fraction of quasiparticles that can tunnel against the bias decreases and the signal increases. Secondly, the density of quasiparticle states in a superconductor diverges at the gap, and decreases over an energy of ~Δ to its normal metal value [14]. For higher bias, the density of states to tunnel into therefore decreases and the signal decreases again. The signal in the Ta-STJs peaks at a lower voltage than in the Nb-STJs, since the energy gap Δ_{Ta} is smaller than Δ_{Nb}.

We have exposed the Ta STJ to X-rays from a Cu target on an Al holder in a two-stage X-ray tube, and processed the signals with a 4 µs Gaussian filter. The spectrum has an energy resolution around ~10 eV FWHM for X-ray energies up to ~1 keV, and increasing slightly at higher energy (Figure 2a). This is comparable to our Nb-STJs, and sufficient to resolve all soft X-rays for fluorescence-detected XAS. Note that the response to C and O K X-rays consists of a single peak, while the Cu L and Al K lines are accompanied by secondary peaks at slightly lower energies due to X-ray absorption in the bottom Ta film. Interestingly, in Ta-STJs these secondary peaks occur at *lower* energies than the main line, as opposed to Nb-STJs where they occur at *higher* energies [8 10]. This is because phonon loss into the Si substrate during the initial charge generation reduces the signal from the bottom electrode, while in Nb-STJs the charge loss into the low-gap NbO surface oxides dominates.

The different thickness d_{Ta} of the two Ta films causes the signal rise times for absorption events in the top and bottom electrode to differ, since the trapping rate into the d_{Al} = 50 nm Al films scales with the fraction of time $d_{Al}/(d_{Al}+d_{Ta})$ that the quasiparticles spend in the Al film while diffusing through the Ta-Al bilayer. X-rays absorbed in the Si substrate produce even slower signals due to the finite photon propagation speed (figure 2b). This can be exploited to improve the spectral purity of the response by selecting only those signals with a rise time <1.1 µs. The resulting spectrum (figure 2c) no longer suffers from the line splitting artifact, and has a lower spectral background between the lines due to the removal of substrate events. This increases the sensitivity for detecting weak X-ray emission lines from dilute samples in XAS at the synchrotron.

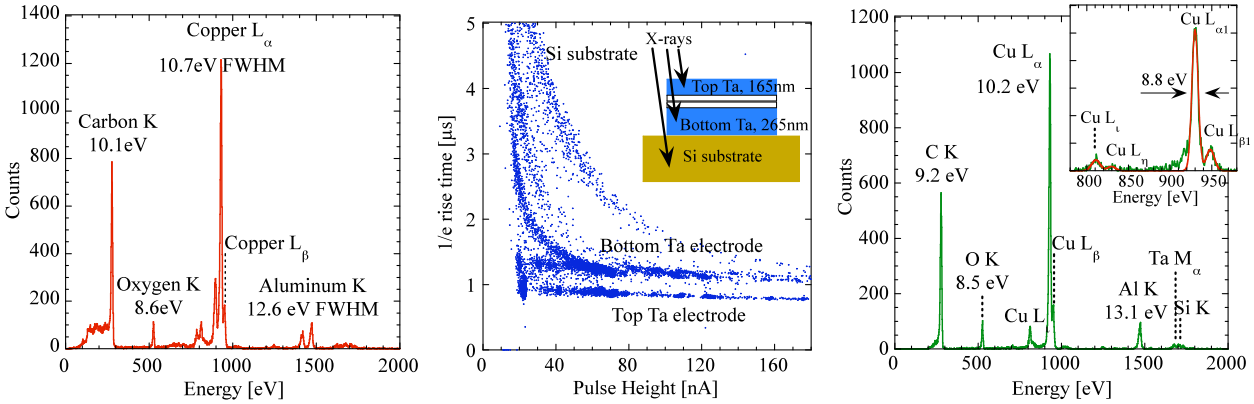

FIGURE 2. (a) Soft X-ray spectrum of a (dirty) Cu target on an Al holder taken with a $(63\ \mu m)^2$ Ta-STJ. (b) The pulse height vs. rise time scatter plot shows that X-rays absorbed in the bottom Ta layer or the Si substrate produce pulses with longer rise times than those absorbed in the top Ta film. (c) Soft X-ray spectrum of the Cu target limited to pulses with a rise time <1.1 µs. The Cu $L_{\alpha1}$ and Al K_α line splitting artifacts at ~900 eV and ~1420 eV, and the substrate events below C K are removed.

DISCUSSION AND OUTLOOK

The fabrication of high-quality Ta-based tunnel junctions is a significant step towards the next generation of STJ soft X-ray spectrometers. Their energy resolution of ~10 eV FWHM for energies up to ~1 keV is already sufficient to effectively separate all elemental soft X-ray fluorescence lines. Their signal decay time of ~30 µs, while ~10× slower than the decay times in our current Nb-STJs [4], should still allow count rates of ~5000 counts/s per pixel, and be sufficient to handle the fluorescence flux at most beam lines, even at 3rd generation synchrotrons.

The use of these Ta STJs at the synchrotron now requires increasing their efficiency. The first step towards this goal is to increase the effective area per pixel without increasing the leakage current. Our current Nb-STJ arrays have $(200\ \mu m)^2$ pixels, limited by the spacing of the Fiske mode resonances, and this should also be attainable for Ta-STJs. Since the devices are fabricated by photolithography, the scaling to arrays is comparably straightforward, and the cryostat for operating 112-pixel arrays has already been built [15]. This would increase the sensitivity for XAS on dilute samples from currently ~hundreds of ppm to ~tens of ppm, depending on the fluorescence yield at the absorption edge under investigation.

Further improvements in detector performance are possible with an increase in Ta absorber film thickness, provided that an associated increase in film stress does not degrade the quality of the tunnel barrier and increase leakage current and noise. In addition, initial experiments at the synchrotron will reveal details of the spectral background between the lines that often determines the detection limits for elements whose emissions are nominally well resolved from the stronger X-ray lines.

ACKNOWLEDGMENTS

This work was funded by the NASA Astrobiology Instrumentation (ASTID) program under grant L-10896. It was performed under the auspices of the U. S. Department of Energy by Lawrence Livermore National Laboratory under Contract DE-AC52-07NA27344.

REFERENCES

1. For an overview of the state-of-the-art in cryogenic detector development, see proceedings of the 12th Intl. Workshop on Low Temperature Detectors (LTD-12), published as *J. Low Temp. Phys*. **151** (2008)
2. S. Friedrich, *J. Synch. Rad*. **13**, 159-171 (2006)
3. J. B. LeGrand et al., *Appl. Phys. Lett*. **73**, 1295-1297 (1998)
4. S. Friedrich et al., IEEE Trans. Appl. Supercond. **13**, 1114-1119 (2003)
5. P. Verhoeve, *J. Low Temp. Phys*. **151**, 675-683 (2008)
6. G. Angloher, P. Hettl, M. Huber, J. Jochum, F. v. Feilitzsch, R. L. Mößbauer, *J. Appl. Phys.* **89**, 1425-1427 (2001)
7. M. Kurakado, *Nucl. Inst. Meth*. **196**, 275-277 (1982)
8. C.A. Mears, S.E. Labov, A.T. Barfknecht, *Appl. Phys. Lett*. **63**, 2961-2963 (1993)
9. K. Segall et al., *Appl. Phys. Lett*. **76**, 3998-4000 (2002)
10. S. Friedrich, L. J. Hiller, M. F. Cunningham, S. E. Labov, *IEEE Trans. Appl. Supercond.* **11**, 836-839 (2001)
11. A. T. Barfknecht, R. C. Ruby, H. Ko, *IEEE Trans. Appl. Magn*. **27**, 3125-3128 (1991)
12. R. Cantor, J. Hall, unpublished
13. J. Jochum, H. Kraus, M. Gutsche, B. Kemmather, *J. Low Temp. Phys*. **93**, 623-630 (1993)
14. A.A. Golubov, E. P. Houwman, V.M. Krasnov, J. Flokstra, H. Rogalla, M.Y.Kupriyanov, *Phys. Rev. B* **51**, 1073-1089 (1995)
15. S. Friedrich, T. Hertrich, O. B. Drury, N. J. Cherepy, J. Höhne, *IEEE Trans. Nucl. Sci.* **56**, 1089-1096 (2009)